

Interlayer cohesive energy of graphite from thermal desorption of polyaromatic hydrocarbonsRenju Zacharia,¹ Hendrik Ulbricht,¹ and Tobias Hertel^{1,2}¹*Department of Physical Chemistry, Fritz-Haber-Institut der Max-Planck-Gesellschaft, Faradayweg 4-6, D-14195 Berlin, Germany*²*Department of Physics and Astronomy, Vanderbilt University, Nashville, Tennessee 37235, USA*

(Received 22 August 2003; published 12 April 2004)

We have studied the interaction of polyaromatic hydrocarbons (PAHs) with the basal plane of graphite using thermal desorption spectroscopy. Desorption kinetics of benzene, naphthalene, coronene, and ovalene at submonolayer coverages yield activation energies of 0.50 eV, 0.85 eV, 1.40 eV, and 2.1 eV, respectively. Benzene and naphthalene follow simple first order desorption kinetics while coronene and ovalene exhibit fractional order kinetics owing to the stability of two-dimensional adsorbate islands up to the desorption temperature. Preexponential frequency factors are found to be in the range 10^{14} – 10^{21} s⁻¹ as obtained from both Falconer-Madix (isothermal desorption) analysis and Antoine's fit to vapor pressure data. The resulting binding energy per carbon atom of the PAH is 52 ± 5 meV and can be identified with the interlayer cohesive energy of graphite. The resulting cleavage energy of graphite is 61 ± 5 meV/atom, which is considerably larger than previously reported experimental values.

DOI: 10.1103/PhysRevB.69.155406

PACS number(s): 81.05.Uw, 61.50.Lt, 68.43.Mn, 81.07.De

I. INTRODUCTION

The cohesive energy of a solid is determined by the interactions among its constituent atoms. In the case of graphite, a layered material with strongly anisotropic bonding, it appears natural to distinguish the total from the interlayer cohesive energy. The first is dominated by strong localized covalent bonding through sp^2 carbon orbitals while the latter is dominated by weak nonlocal van der Waals (vdW) interactions between graphene sheets. A description of the cohesive energy of graphite thus necessarily involves interactions of fundamentally different character and poses a true challenge even to the most advanced calculational techniques. In particular, dispersion forces that give rise to the long-range attraction between graphene layers have been notoriously difficult to predict. Not too surprisingly, one finds that values calculated from semiempirical or *ab initio* methods for the interlayer cohesive or exfoliation energy of graphite range from as little as 8 meV/atom up to 170 meV/atom.^{1–6} Experimental determinations of the interlayer cohesive energy of graphite have been comparatively rare and are restricted to a heat of wetting experiment by Girifalco which yields an exfoliation energy of 43 meV/atom^{7,8} and a measurement by Benedict *et al.* based on radial deformations of multiwall carbon nanotubes which yields 35 meV/atom.⁹ At this point it seems that not only the agreement between theory and experiment leaves room for improvement but that the experimental evidence for such comparisons should also be put on a firmer basis.

Here, we aim at a better experimental characterization of the weak interlayer interactions in graphite using thermal desorption of thin films of polyaromatic hydrocarbons from the surface of a highly oriented pyrolytic graphite (HOPG) sample. Polyaromatic hydrocarbons (PAHs) are planar aromatic molecules formed by two or more fused aromatic rings and valencies of peripheral atoms are satisfied through covalent bonded hydrogen atoms. The interaction of PAHs with graphite is thus considered as suitable model system for the interaction between graphene layers. This analogy is also

supported by their striking structural resemblance, i.e., the same hybridization of atoms and practically identical bond lengths as well as the formation of adsorbate layers commensurate with the substrate^{10–12} which suggests that the character of the interaction between PAHs and graphite—in particular for larger PAHs—should be the same as that of the interaction of a graphene sheet with a graphite substrate. Moreover, the electronic structure and density of states of larger PAHs converges rapidly to that of graphene.¹⁵

A better understanding of the long-range vdW forces in graphitic systems is also of interest when interactions between carbon nanotubes (CNTs) are studied, for example. The latter are frequently found to be agglomerated in so-called carbon nanotube ropes, quasicrystalline arrangements of close packed CNTs which are difficult to separate due to considerable long-range vdW interactions.¹³ Only recently have soaps been successfully used to separate and exfoliate such ropes,¹⁴ where again vdW forces between the surfactant and the tubes play a crucial role as for the wider field of soft matter physics.

II. EXPERIMENT

Thermal desorption (TD) experiments were performed under ultrahigh-vacuum (UHV) conditions where the base pressure of below 1×10^{-10} mbar was maintained using a combination of membrane, turbodrag, and turbomolecular pumps. The HOPG sample from Advanced Ceramics (Grade ZYB) was mounted on a Ta disk using conducting silver epoxy and was freshly cleaved prior to transfer into the vacuum chamber. The sample surface was cleaned prior to dosing by repeated annealing cycles to 1200 K. A type-K thermocouple was spot welded to the Ta disk to measure and allow control of the sample temperature. The thermocouple was calibrated using desorption of Xe multilayers in combination with their well known heat of sublimation. The sample holder was attached to a He continuous flow cryostat that enabled sample cooling down to 30 K.

Benzene or naphthalene (99.89% and 99.99%, Aldrich)

vapor was admitted from a gas reservoir to the sample surface through a retractable pinhole doser. Unwanted atmospheric contaminants were removed from the solvents by freeze-pump cycles prior to adsorption experiments. Exposure of HOPG to coronene (99%, Aldrich) and ovalene (99.5%, Dr. Ehrenstorfer GmbH) was by sublimation of powder material from a PID temperature controlled Knudsen cell. A typical coverage series of TD traces was obtained by dosing the graphite surface with successively increasing adsorbate quantities up to a total coverage of approximately 5 monolayers (ML). TD spectra were recorded for a constant heating rate between 0.75 K/s and 2 K/s. Desorption of species with a mass to charge ratio of up to 200 amu/e, such as benzene and naphthalene, could be monitored using a quadrupole mass spectrometer (Spectra Satellite). Due to their high molecular mass, coronene and ovalene desorption signals had to be obtained from the total pressure inside the UHV chamber as monitored by a Bayard-Alpert ionization gauge. Background correction of the latter TD traces was carefully cross-checked with simultaneously recorded TD spectra from species with masses between 4 and 200 amu. Further details of the experimental procedure are available elsewhere.¹⁶

III. RESULTS AND DISCUSSION

A. Thermal desorption of PAHs

We begin our discussion with benzene TD spectra shown in Fig. 1(a), which were recorded after exposure of the HOPG surface with a dose of up to 5 L (1 L = 1×10^{-6} Torr s). The TD spectra are characterized by a high temperature feature attributed to desorption from the first monolayer and a low temperature feature due to the desorption from multilayers, which are centered around 152 K and 142 K, respectively. The submonolayer phase diagram of benzene on graphite shows a complex pattern of phase transitions wherein the high coverage and high temperature phases benzene molecules tend to be oriented with their molecular plane perpendicular to the graphitic surface to satisfy steric and entropic constraints.¹⁷ However, at coverages significantly below 1 ML and at 152 K, i.e., the temperature of desorption in our experiments, the molecules are expected to be adsorbed with their aromatic rings parallel to the surface.¹⁷ The shape of TD spectra and the coverage independent desorption peak maximum at low coverages are clearly indicative of first-order kinetics. With coverages approaching the monolayer regime, however, the desorption traces broaden toward the low temperature side and become more complex—as expected due to the changes of molecular orientation within the adsorbate layer at higher coverages. The TD spectrum from a complete monolayer is here associated with the last trace before the additional desorption feature around 140 K develops with increasing coverage. The latter is typical of desorption from multilayers with a common leading edge corresponding to zero-order kinetics.

As in the case of benzene, the coverage series for naphthalene desorption exhibits two clearly distinguishable desorption features corresponding to mono- and multilayer desorption, respectively [see Fig. 1(b)]. The TD spectra of

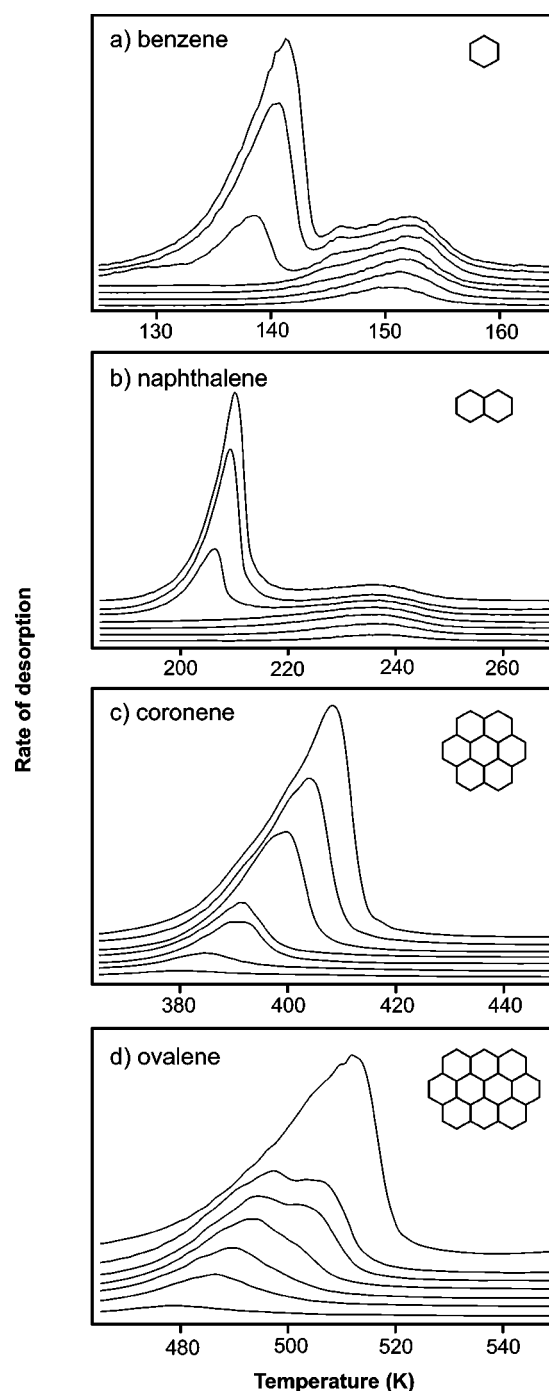


FIG. 1. Series of thermal desorption spectra from the HOPG surface. Coverages in parentheses are given in units of close-packed monolayers for (a) benzene (0.4,0.6,0.8,1.0,2.3,4.0,5.1), (b) naphthalene (0.3,0.6,0.8,1.0,2.2,3.9,4.8), (c) coronene (0.1,0.5,0.8,1.0, 2.4,3.6,5.1), and (d) ovalene (0.2,0.5,0.8,1.0,1.4,1.8,2.9). The rate of desorption was 0.7 K s⁻¹, 1.0 K s⁻¹, 2.0 K s⁻¹, and 2.0 K s⁻¹, respectively.

coronene and ovalene in Figs. 1(c) and 1(d) on the other hand do not exhibit clearly distinguishable mono- and multilayer desorption features. At low exposure, desorption traces from both substances exhibit a behavior indicative of fractional order kinetics. Here, the saturation of the first monolayer is estimated from the onset of multilayer desorp-

tion as apparent from the development of a common leading edge in the TD spectra at higher coverages. This leaves us with considerable uncertainty of the actual monolayer coverage which—as a worst case scenario—is assumed to be at most a factor of 2 higher or smaller. For ovalene, further evidence for the formation of the first monolayer is obtained from the appearance of a shoulder in the TD spectra before the common leading edge develops. The monolayer desorption maxima for coronene and ovalene are found at 390 K and 490 K, respectively. Adsorption of coronene monolayers on graphite reportedly also leads to the formation of two-dimensional (2D) islands¹² owing to lateral interaction between adsorbed molecules, which in the case of coronene and ovalene may make islands stable up to typical desorption temperatures. Under such circumstances, diffusion from the island edges may become rate limiting and give rise to fractional order desorption kinetics as observed for coronene and ovalene (see analysis in the next section).

B. Determination of frequency factors and binding energies

The rate of desorption of some adsorbate from a solid surface is commonly described by an Arrhenius equation:

$$\frac{d\theta}{dt} = -\nu\theta^n \exp(-E_a/k_B T) \quad (1)$$

where ν is the preexponential frequency factor, θ is the surface coverage, and E_a is the activation energy for desorption.

In the following we will determine the activation energies for desorption of each adsorbate using the series of TD traces presented above. Based on the above Arrhenius equation, a variety of techniques, each one with unique merits, can be used to obtain activation energies. Here, we will focus on an analysis using Redhead's peak maximum method¹⁸ and an isothermal analysis introduced by Falconer and Madix.¹⁹

1. Redhead analysis

The Redhead equation¹⁸ relates E_a , the temperature at the desorption peak maximum T_{\max} , and the heating rate β as follows:

$$E_a = k_B T_{\max} [\ln(\nu T_{\max} / \beta) - 3.64]. \quad (2)$$

The use of the latter expression is most commonly applied to systems with first-order kinetics but can be extended to fractional or zero-order kinetics if the desorption trace used for determination of T_{\max} corresponds to evaporation from a saturated monolayer.

A crucial factor for the analysis of TD spectra using Redhead's peak maximum method is the availability of reliable preexponentials. Commonly, the latter are assumed to be on the order of 10^{13} – 10^{15} s⁻¹ and small uncertainties of less than an order of magnitude will not give rise to any serious error of the activation energy. However, the assumption of constant preexponentials is sometimes problematic,²⁰ in particular if large adsorbates with many internal degrees of freedom are studied.²¹ For thermal desorption of alkane chains from graphite, for example, preexponential factors have been calculated using transition state theory (TST) and were found

to increase by over four orders of magnitude with chain length from 10^{12} s⁻¹ for methane up to 10^{16} s⁻¹ for C₁₂H₂₆.²¹ Qualitatively this can be attributed to constraints on various vibrational degrees of freedom of the molecule in the adsorbed state. If preexponentials are calculated from TST one generally computes the ratio of partition functions in the adsorbed and the transition state. If molecular degrees of freedom are somewhat constrained or “frozen in” in the adsorbed state this will usually reduce the corresponding partition function and thus tends to give higher preexponential factors. When studying and analyzing the thermal desorption of small and larger polyaromatic compounds we will thus avoid using estimated preexponentials and instead use experimentally determined values.

We here assume that preexponential frequency factors do not depend strongly on the film thickness and that multilayer values can thus also be used for analysis of monolayer desorption traces. Preexponentials for multilayer desorption can be obtained using the temperature dependence of the adsorbate vapor pressure. This is done by assuming detailed balance between the rate of adsorption and desorption between a multilayer film in equilibrium with its gas-phase vapor. A similar approach has previously been used by Schlichting and co-workers.²² The preexponential frequency factor can then be expressed as

$$\nu = \frac{s}{\sigma \sqrt{2\pi m k_B T}} p_0, \quad (3)$$

where s is the sticking coefficient, σ the number of adsorbates per unit area, m their mass, and p_0 the vapor pressure at infinite temperature. The latter is obtained from the temperature dependence of the vapor pressure using

$$p(T) = p_0 \exp\left(-\frac{\Delta H_s}{k_B T}\right). \quad (4)$$

Here, ΔH_s is the heat of sublimation at the temperature of desorption T_{\max} . However, none of the vapor pressure curves reported in the literature extend to the range of desorption temperatures in these experiments.^{23–25} Due to the commonly observed increase of ΔH_s with decreasing temperature we thus have to extrapolate and evaluate the vapor pressure curves at temperatures where desorption occurs in our experiments. This can be done by a fit to vapor pressure data using Antoine's expression:²⁶

$$\ln[p(T)] = A - \frac{B}{T+C}, \quad (5)$$

where A , B , and C are the fit coefficients listed in Table I.

For ovalene, where no vapor pressure data are available, the preexponential factor 5.6×10^{21} s⁻¹ was obtained using the tabulated slope and offset from the Clausius-Clapeyron equation in the form $\ln(p) = A - B/T$.²⁵ The density σ of benzene, naphthalene, and coronene molecules adsorbed on the graphite surface can be obtained from low energy electron diffraction or scanning tunneling microscopy data.^{12,27} For ovalene where again no such data are available σ can be

TABLE I. Vapor pressures and desorption temperatures used to compute the frequency factor.

Molecule	A	B (K)	C (K)	σ (cm ⁻²) ^a	p_0 (mbar)	T_{\max} (K)
Benzene	26	7640	30	2.7×10^{18}	5.8×10^{11}	151
Naphthalene	43	20 100	124	1.6×10^{18}	1.3×10^{14}	235
Coronene	37	30 400	184	0.9×10^{18}	2.6×10^{13}	390
Ovalene				0.6×10^{18}	7.6×10^{13}	490

^aSee the text for references.

estimated assuming that molecules are close packed with the polyaromatic rings oriented parallel to the surface. The resulting densities are summarized in Table I.

The sticking coefficient s used in Eq. (3) is here assumed to be close to unity, which is commonly observed for homoepitaxial growth and should also be appropriate for adsorption of weakly interacting polyaromatics on graphite. Table I summarizes all parameters used for the computation of frequency factors as well as the temperature at the desorption peak maximum used for computation of the activation energy from the Redhead equation. The computed frequency factors are summarized in Table II together with the resulting activation energies as obtained from Eq. (2).

2. Falconer-Madix analysis

In this section we will perform an isothermal analysis of TD spectra of the type frequently referred to as the Falconer-Madix method.¹⁹ For this purpose we plot the logarithm of the desorption rate $\ln(-d\theta/dt)$ versus $\ln \theta$ as evaluated at one specific temperature for several desorption traces of different initial coverage. A linear fit to the resulting data sets from submonolayer coverages as shown in Fig. 2 can be analyzed according to

$$\ln\left(-\frac{d\theta}{dt}\right) = \ln \nu + n \ln \theta - \frac{E_a}{k_B T}. \quad (6)$$

If the intercept I

$$I = \ln(\nu) - \frac{E_a}{k_B T} \quad (7)$$

is plotted versus $1/T$ (see Fig. 3 for naphthalene) one obtains the preexponential frequency factor as well as the activation energy from a straight line fit to the data. From the slope of naphthalene and benzene desorption isotherms we obtain the order of desorption n of 0.95 ± 0.02 and $n = 1.01 \pm 0.02$, re-

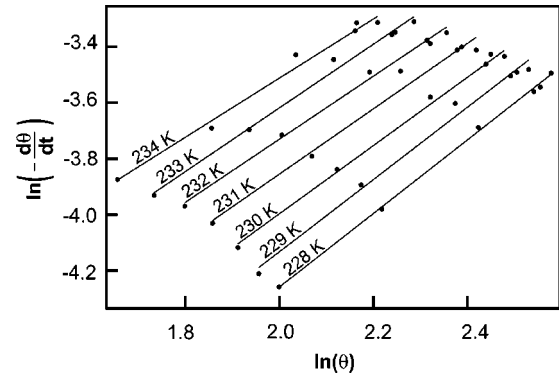


FIG. 2. Linear fit to isothermal desorption data for naphthalene in the temperature range of 228 to 234 K.

spectively. On the other hand, coronene and ovalene appear to follow fractional order kinetics with $n = 0.27 \pm 0.04$ and 0.34 ± 0.01 , respectively.

The preexponentials as well as the activation energies obtained from this analysis are summarized together with the results from the Redhead peak-maximum analysis in Table II.

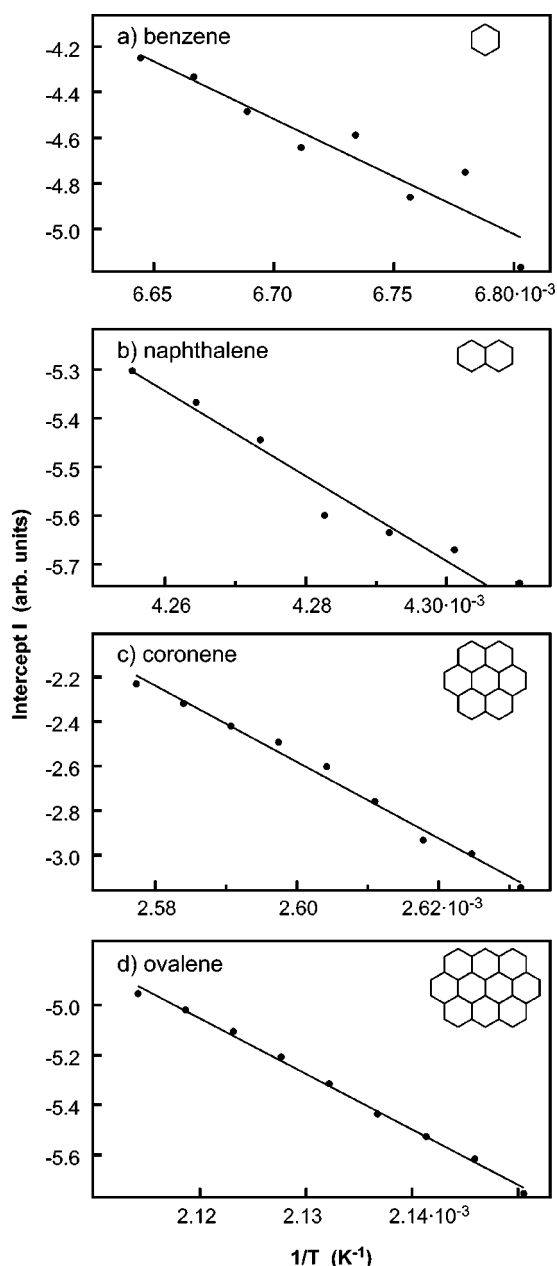
Note, that the preexponential frequency factors in the present study are considerably larger than those commonly used for desorption of smaller molecules where typical values are on the order of 10^{13} s^{-1} to 10^{15} s^{-1} . This reinforces the necessity to determine these parameters accurately and reliably either from experiments or by complementary theoretical investigations as recently reported by Fichthorn *et al.*²¹ The high preexponentials found here can qualitatively be accounted for by the larger difference between partition functions in the adsorbed and the transition states, if compared with desorption of mono- or diatomic adsorbates, for example. A comparison of the preexponentials obtained here by the two different methods shows good agreement within estimated error bars.

C. The interlayer cohesive energy of graphite

The cohesive energy of a solid is commonly referred to as the energy needed to “disassemble it into its constituent parts”²⁸ while the work of cohesion is occasionally also referred to as the energy needed to “separate unit areas...” of a medium “...from contact to infinity in vacuum.”²⁹ The two are not identical and for a layered system with extremely anisotropic bonding like graphite the first can be identified with the exfoliation energy E_{ex} , i.e., the energy

TABLE II. Binding energy and frequency factor: comparison between Redhead and Falconer-Madix analysis.

	Redhead		Falconer-Madix	
	ν (s ⁻¹)	E_a (eV)	ν (s ⁻¹)	E_a (eV)
Benzene	$1 \times 10^{16 \pm 3}$	0.50 ± 0.08	$5.0 \times 10^{15 \pm 2}$	0.50 ± 0.08
Naphthalene	$5 \times 10^{16 \pm 2}$	0.8 ± 0.1	$1.0 \times 10^{17 \pm 1.5}$	0.90 ± 0.07
Coronene	$2 \times 10^{16 \pm 2}$	1.3 ± 0.2	$1.7 \times 10^{18 \pm 0.5}$	1.5 ± 0.1
Ovalene	$5 \times 10^{21 \pm 3}$	2.2 ± 0.2	$8.0 \times 10^{18 \pm 0.5}$	1.97 ± 0.08

FIG. 3. Plot of intercept I vs inverse temperature.

needed to separate all layers of the crystal to infinity, while the latter is equivalent to the cleavage energy E_{c1} , which is commonly slightly larger than the exfoliation energy. Previous work suggests that the energy needed to separate a single sheet of graphene from a graphite crystal, i.e., the exfoliation energy, is approximately 18% smaller than the cleavage energy.⁸ The normalization in this paper will be with respect to surface atoms and not to area. The area per surface atom in a graphene sheet is $[(2.46 \times 10^{-10} \text{ m})^2 \times \sqrt{3}] = 1.05 \times 10^{-19} \text{ m}^2$.

In the following we will use the results from the previous section to determine the interlayer cohesive energy of graphite to which the dominant contribution is generally believed to arise from long-range van der Waals interactions between graphene sheets. Our approach for the determination of the

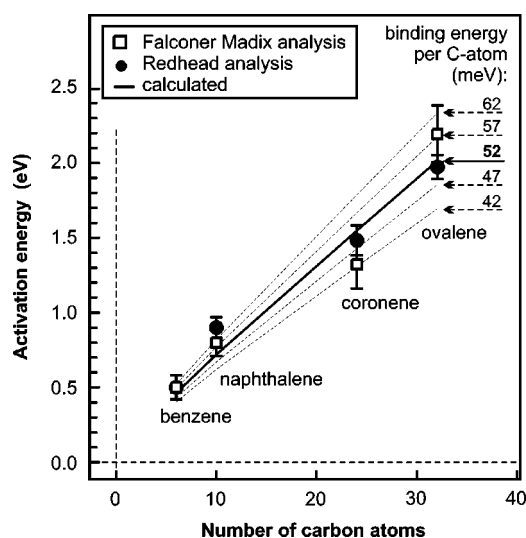


FIG. 4. Dependence of activation energy for desorption on the number of carbon atoms of four polyaromatic hydrocarbons.

interlayer cohesive energy—using the activation energies for desorption of small polyaromatic molecules, i.e., small “flakes of graphene”—is based on the near-additivity of such vdW interactions.^{29,30} The latter is well established, for example, for the cohesive energy of alkanes where deviations from linearity in the number of chain segments are about 1% or less.²⁹ The activation energy for desorption—as measured by TD spectroscopy—will here be identified with the binding energy of the adsorbate to the graphite surface. The contribution of individual carbon atoms to this binding energy is derived from our data which—in the limit of infinitely large PAHs—would correspond to the energy needed to separate a graphene sheet from its parent crystal and is thus associated with the interlayer cohesive energy. Additional contributions to the desorption energy from intermolecular interactions are assumed to be negligible. This is justified if adsorbate-adsorbate interactions are either small due to large mutual separation—as in the case of the low coverage regime for benzene or naphthalene desorption—or this may be justified if adsorbate-adsorbate interactions within 2D islands on the surface are comparatively small as in the case of adsorbed coronene or ovalene.

A rough estimate of the exfoliation energy can be obtained by averaging over desorption energies per carbon atom for all studied adsorbates, which would yield 67 meV/atom. In this case, however, one neglects the small but significant contribution to the binding energy from hydrogen atoms and this approach is thus expected to overestimate the contribution of carbon atoms to the total binding energy. A more thorough analysis of the binding energies plotted in Fig. 4 thus also has to account for the contribution of hydrogen atoms. Here, this is done by optimizing the carbon-carbon and hydrogen-carbon interaction potentials to give optimum agreement of experimental energies with calculated binding energies. Experimental data for this optimization are averaged over values obtained from both the peak maximum and isothermal analysis. The calculated binding energies are obtained in the usual manner by summation over empirical vdW pair potentials:

$$E_B^{\text{PAH}} = \sum_{n,m} V^{\text{CC}}(|r_n - r_m|) + \sum_{l,m} V^{\text{HC}}(|r_l - r_m|), \quad (8)$$

where the summation over n and l includes all carbon or hydrogen atoms in the adsorbate and the summation over m includes all atoms in the substrate. The carbon-carbon (C-C) and carbon-hydrogen (C-H) vdW potentials are those of the MM3 force field by Allinger and co-workers.³¹ They have the form

$$V^{AB}(r) = \epsilon_{AB} \left[184\,000 \exp\left(-\frac{12r}{r_{AB}}\right) - 2.25 \left(\frac{r_{AB}}{r}\right)^6 \right], \quad (9)$$

where for dissimilar atoms A and B ϵ_{AB} is given by $\epsilon_{AB} = \sqrt{\epsilon_A \epsilon_B}$ and r_{AB} is given by $r_{AB} = r_A + r_B$. The values (ϵ_C, r_C) and (ϵ_H, r_H) given by Allinger and co-workers for carbon and hydrogen are $(2.44 \text{ meV}, 1.96 \text{ \AA})$ and $(0.87 \text{ meV}, 1.67 \text{ \AA})$, respectively. In the following we use the depth of the two vdW potentials V_0^{CC} and V_0^{HC} as free scalable parameters while the position of the potential minima is kept fixed. The binding energy $E_B^{\text{PAH}}(V_0^{\text{CC}}, V_0^{\text{HC}}, z)$ is then optimized by adjusting the molecule-surface distance z while the orientation of the aromatic rings of the molecules is fixed parallel to the graphite surface. We then determine the set of parameters V_0^{CC} and V_0^{HC} which gives best simultaneous agreement of all calculated with all experimental binding energies by minimizing the corresponding root mean square deviation. Using the MM3 force field parameters the depth of the hydrogen vdW potential for interaction with a graphite surface is estimated to be 27 meV/atom. If we allow this to vary by at most ± 5 meV, we get best agreement with the experimental binding energies if the depth of the carbon-graphite potential is 52 ± 5 meV/atom. From Fig. 4, where calculated and experimental binding energies are compared, one finds that deviations between experimental and calculated values are about 10% or less. The major uncertainty here arises due to the large error bars of the preexponential in the Redhead method and from the estimated error of the temperature calibration as well as the reproducibility of TD traces due to small variations of the sensed temperature for the Falconer-Madix analysis. For coronene and ovalene an additional error of about 2% arises due to uncertainties of the coverage calibration. The cleavage energy of graphite is obtained from the above value by accounting for the 18% higher energy previously observed for the separation of two crystal halves if compared with the separation of a single graphene layer from its parent crystal.⁸ This yields a cleavage energy of 61 ± 5 meV/atom which is significantly larger than previously reported values.

The earliest measurement of the exfoliation energy from heat of wetting experiments by Girifalco and Lad gave 260 ± 30 ergs/cm² which—using the carbon atom density within a graphene sheet—is equivalent to 43 ± 5 meV per surface atom.⁸ Unfortunately, the only documentation for the heat of wetting data used for the determination of E_{ex} by Girifalco and Lad has been published in a thesis and is not readily available.^{7,8} Also, no information on the kind of graphite sample used in the original experiments is available. Carbon powders commonly used for such experiments usually have

higher surface areas of the order of tens to hundreds of square meters per gram. They are usually treated with acids to oxidize nongraphitic contaminants and are then thermally treated to achieve the highest possible degree of graphitization. The adsorptive properties and surface chemistry of such carbons, however, depend strongly on the history of the sample treatment.³² An assessment of systematic and sample dependent uncertainties of the value reported by Girifalco is thus difficult.

An even smaller value of 35_{-10}^{+15} meV/atom for the cohesive energy of graphite was obtained by Benedict *et al.* from the analysis of collapsed multiwall carbon nanotubes.⁹ This analysis is based on a measurement of the diameter of hollow “bulbs” at the sides of three different collapsed multiwall carbon nanotubes with a precision of about 1–2 Å. Other than statistical errors or those due to the limited accuracy of the bulb diameter determination may also contribute to uncertainties associated with this value. This again makes it difficult to assess the relevance of possible systematic or statistical errors which could help to better understand the discrepancy between our and other experimental determinations of the cohesive energy of graphite. Note that a distinct advantage of the present investigation is that the experimental conditions and assumptions leading to the conclusions are most clearly defined and that a well characterized model system is used for the investigation of the interlayer cohesive energy of graphite.

As stated in the Introduction, theoretical estimates using *ab initio* or semiempirical methods show a much stronger variation from values as little as 8 meV/atom to as much as 170 meV/atom.^{1–6} These large discrepancies are partly due to the inherent difficulties encountered in the calculation of long-range dispersion forces. Even advanced calculations using nonlocal density functional theory,⁶ which account for vdW interactions, with reported values for a single pair of graphene sheets of only 35 meV/atom tend to underestimate the interlayer cohesive energies. However, the desorption energies reported here for different PAHs may serve as a useful benchmark for future studies to allow a better comparison of theoretical binding energies with experiment. Reliable values for the cleavage and interlayer cohesive energies may eventually be derived from a successful calculation of the interaction of PAHs with graphite if the interlayer forces in graphite can be treated on the same footing.

IV. SUMMARY

In conclusion, we have presented a thermal desorption study of benzene, naphthalene, coronene, and ovalene adsorbed on the basal plane of graphite. Binding energies were obtained by the peak-maximum method and alternatively by an isothermal analysis which also allowed us to determine preexponential frequency factors. For the peak-maximum method we derived preexponentials from vapor pressure data in combination with Antoine’s law for extrapolation of the data to the temperature of desorption. Both methods indicated that preexponential factors increase with adsorbate size from 10^{14} s^{-1} to 10^{21} s^{-1} . The corresponding binding energies increase from 0.50 eV for benzene to 2.1 eV for

ovalene. These values were used to determine the interlayer contribution to the cohesive energy of graphite by assuming pairwise additivity of the interaction of carbon and hydrogen atoms to the total binding energy of the molecules. The resulting cleavage energy of graphite of 61 ± 5 meV/atom is derived from the average carbon atom contribution to the binding energy of the PAHs of 52 ± 5 meV/atom, which can also be associated with the exfoliation energy. This is significantly larger than previous experimental determinations, and

these results provide an experimental benchmark for future theoretical investigations of interlayer bonding and van der Waals interactions in graphitic systems.

ACKNOWLEDGMENT

It is our pleasure to acknowledge continuing support by G. Ertl.

-
- ¹R. O. Brennan, *J. Chem. Phys.* **20**, 40 (1952).
²N. L. Allinger, *J. Am. Chem. Soc.* **99**, 8127 (1977).
³Matthias C. Schabel and José Luís Martins, *Phys. Rev. B* **46**, 7185 (1992).
⁴S. B. Trickey, F. Müller-Plathe, G. H. F. Diercksen, and J. C. Boettger, *Phys. Rev. B* **45**, 4460 (1992).
⁵J. Ch. Charlier, X. Gonze, and J.P. Michenaud, *Europhys. Lett.* **28**, 403 (1994).
⁶H. Rydberg, N. Jacobson, P. Hyldgaard, S. I. Simak, B. I. Lundqvist, and D. C. Langreth, *Surf. Sci.* **532**, 606 (2003).
⁷L. A. Girifalco, Ph.D. thesis, University of Cincinnati, 1954.
⁸L. A. Girifalco and R. A. Lad, *J. Chem. Phys.* **25**, 693 (1956).
⁹Lorin X. Benedict, Nasreen G. Chopra, Marvin L. Cohen, A. Zettl, Steven G. Louie, and Vincent H. Crespi, *Chem. Phys. Lett.* **286**, 490 (1998).
¹⁰I. Gameson and T. Rayment, *Chem. Phys. Lett.* **123**, 150 (1986).
¹¹U. Zimmermann and N. Karl, *Surf. Sci.* **268**, 296 (1992).
¹²Karsten Walzer, Micheal Sternberg, and Micheal Hietschold, *Surf. Sci.* **415**, 376 (1998).
¹³A. Thess, R. Lee, P. Nikolaev, H. J. Dai, P. Petit, J. Robert, C. H. Xu, Y. H. Lee, S. G. Kim, A. G. Rinzler, D. T. Colbert, G. E. Scuseria, D. Tomanek, J. E. Fischer, and R. E. Smalley, *Science* **273**, 483 (1996).
¹⁴M. J. O'Connell, S. M. Bachilo, C. B. Huffman, V. C. Moore, M. S. Strano, E. H. Haroz, K. L. Rialon, P. J. Boul, W. H. Noon, C. Kittrell, J. Ma, R. H. Hauge, R. B. Weisman, and R. E. Smalley, *Science* **279**, 593 (2002).
¹⁵Henna Ruuska and Tapani A. Pakkanen, *J. Phys. Chem. B* **105**, 9541 (2001).
¹⁶Hendrik Ulbricht, Jennah Kriebel, Gunnar Moos, and Tobias Hertel, *Chem. Phys. Lett.* **363**, 252 (2002).
¹⁷Peter Meehan, Trevor Rayment, Robert K. Thomas, Guillermo Bomchil, and John W. White, *J. Chem. Soc., Faraday Trans. 1* **76**, 2011 (1980).
¹⁸P. A. Readhead, *Vacuum* **12**, 203 (1962).
¹⁹John L. Falconer and Rober J. Madix, *J. Catal.* **48**, 262 (1977).
²⁰Kris R. Parseba and Andrew J. Gellmann, *Phys. Rev. Lett.* **86**, 4338 (2001).
²¹Kristen A. Fichthorn and Radu A. Miron, *Phys. Rev. Lett.* **89**, 196103 (2002).
²²Hartmut Schlichting, Ph.D. thesis, Technische Universität, München, 1990.
²³C. G. De Kruif, *J. Chem. Thermodyn.* **12**, 243 (1980).
²⁴Vahur Oja and Eric M. Suuberg, *J. Chem. Eng. Data* **43**, 486 (1998).
²⁵Hirro Innokuchi, Sukekuni Shiba, Takashi Handa, and Hideo Akamatu, *Bull. Chem. Soc. Jpn.* **25**, 299 (1952).
²⁶Ch. Antoine, *C. R. Hebd. Seances Acad. Sci.* **107**, 681 (1888).
²⁷U. Bardi, S. Magnanelli, and G. Rivoda, *Langmuir* **3**, 159 (1987).
²⁸N. W. Ashcroft and N. D. Mermin, *Solid State Physics* (Saunders Company, Philadelphia, 1976).
²⁹Jacob Isrealachvilli, *Intermolecular and Surface Forces*, 2nd ed. (Academic Press, London, 1992).
³⁰Jenn-Heui Lii and Norman L. Allinger, *J. Am. Chem. Soc.* **111**, 8576 (1989).
³¹N. L. Allinger, Y. H. Yuh, and J.-H. Lii, *J. Am. Chem. Soc.* **111**, 8551 (1989).
³²R. Schlögl, *Handbook of Porous Solids* (Wiley-VCH, Weinheim, 2002), p. 1863.